Supporting information for Decomposition pathways of isoprene-derived hydrotrioxides and their clustering in the atmosphere

Emelda Ahongshangbam, Lauri Franzon, Thomas Golin Almeida, Galib Hasan, Benjamin N. Frandsen, Nanna Myllys

Benchmarking of computational methods: Detailed balance approach

Another way to benchmark the accuracy of our computations is to use the experimental decomposition rate of 1.1×10^{-4} s^{-1} at 300 K with a temperature-dependence of $k(T) \approx 1.9 \times 10^{10} T^{1.35} \exp\left(-\frac{12000\text{ K}}{T}\right)$ s^{-1} provided by Assaf *et al.*[1]. Seeing which of the decomposition energies in Table 2 (in main text) is able to best reproduce this value would provide additional hints as to where the observed systematic error in the decomposition energies comes from. Computational decomposition rates were determined using canonical detailed balance:

$$k_d = k_a \frac{[\text{RO}][\text{HO}_2]}{[\text{ROOOH}]} = k_a \frac{p}{k_B T} \exp\left(\frac{G_{\text{ROOOH}} - G_{\text{HO}_2} - G_{\text{RO}}}{k_B T}\right) \tag{1}$$

where $\frac{p}{k_B T}$ is the ideal gas concentration, G_X are the Gibbs free energies of the system X, and k_a is the association rate of the two radicals, which was calculated using the Long-Range Transition State Theory dipole-dipole capture rate[2] (presented in atomic units as in the source):

$$k_a = \frac{C}{\sqrt{\mu}} (d_{\text{HO}_2} d_{\text{RO}})^{\frac{2}{3}} T^{-\frac{1}{6}} \tag{2}$$

where C is a constant provided by Georgievskii and Klippenstein[2], $\mu = \frac{m_{\text{RO}} m_{\text{HO}_2}}{m_{\text{RO}} + m_{\text{HO}_2}}$ is the reduced mass, and d_X are the dipole moments. Values for the dipole moments used were $d_{\text{HO}_2} = 2.20020$ Debye and $d_{\text{RO}} = 2.07234$ Debye, determined using using B3LYP[3]/aug-cc-pVTZ, which has been proved to be a reliable method when it comes to dipole moments.[4] The resulting association rate at 300 K was $k_a = 4.92 \times 10^{-10}$ cm^3 molecule^{-1} s^{-1}. The T-dependence of the Gibbs free energy for each individual system may be expressed as $G(T) = E + k_B T(1 - \ln Q(T))$, where the M06-2X list of frequencies was used for the T-dependence of the partition functions Q at all levels of theory, as this quantity is only a negligible source of error. The resulting decomposition rates are presented in Figure S1.

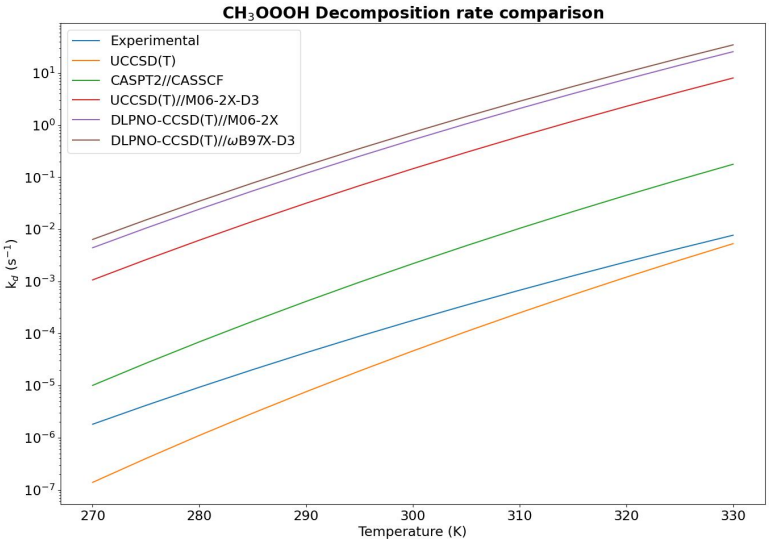

Figure S1: Comparison of the Assaf *et al.*[1] experimental $k_d(T)$ with detailed balance rates calculated using the UCCSD(T) and CASPT2(14,12) energies from Berndt *et al.*[5], the UCCSD(T)//M06-2X-D3 energies from Müller *et al.*[6] and our DLPNO//DFT energies.

Proposed decomposition channel of isoprene-derived hydrotrioxides.

We also investigate an alternative decomposition channel pathway, say pathway (3) which involves the cleavage of the oxygen-oxygen bond of trioxide moiety and subsequent transfer of the -OOH group to the nearest carbon center followed by intra-molecular hydrogen shift to form R(OH)(OOH) as seen in the Figure S2. The intermediate [R-(OH)(OHO)] generated in the pathway possesses two opposite charges and is more stable than their respective reactant system. It is noteworthy to mention that among all the isoprene-derived hydrotrioxides investigated, only three isomers namely; R^1-OOOH, R^4-OOOH and R^5-OOOH as well as methyl-trioxide CH_3OOOH exhibit to undergo this decomposition channel which was confirmed by the IRC calculations. While the rest of the isomers deviate to form respective products with C=O complexes and hydrogen peroxides (H_2O_2), their initial barrier heights are found to be extremely large. Therefore, we abstain from further calculation for this particular mechanism in this study.

$$\mathrm{ROOOH} \longrightarrow \mathrm{R(OH)(OHO)} \tag{3}$$

$$\mathrm{R(OH)(OHO)} \longrightarrow \mathrm{R(OH)(OOH)} \tag{4}$$

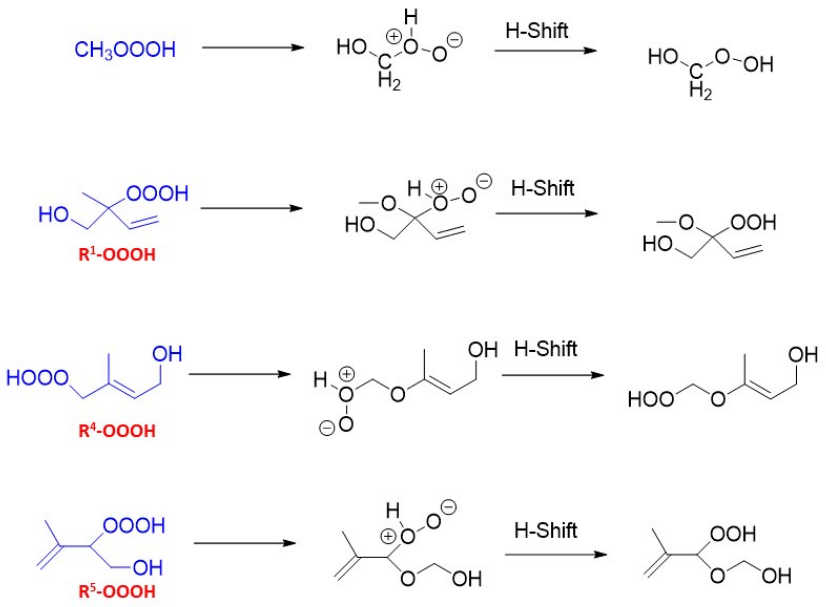

Figure S2: Proposed decomposition mechanism (3) of selected isomers of isoprene derived hydrotrioxides.

Table S1 provides the barrier energies (TS - reactant), reaction energy (final product - reactant), and unimolecular rate coefficients of both the pathway (3.1) and pathway (3.2). The energetics were calculated in the same workflow as described in the method section of the main text at the ωB97X-D/6-31+G* and single-point energy corrections at the DLPNO-CCSD(T)/aug-cc-pVTZ level. For investigating the rates, we employed traditional transition state theory with a quantum-chemical tunneling coefficient taking into account (the equation given in the main text). As we can see from Table S1, the barriers to form the intermediate (first step itself) are so high, although the subsequent intramolecular H-transfer is quite fast. This infers that the reaction is unlikely to occur in the gas phase, however, perhaps the reaction could catalyzed in an aqueous phase or in a particle surface. On top of this pathway, it is worth noting that we briefly calculated ring-closing reactions of isoprene-derived hydrotrioxide (in particular, R^1-OOOH) proceeding via intra-molecular H-shift transfer to form either five or six-membered ring structures at DFT level theory. Preliminary results indicate that this is infeasible in the atmosphere, due to extremely high energy barriers. Therefore, we cease to investigate from further study nor present its energetics in this manuscript.

Table S1: Zero-point energy corrected energy barriers (ΔE^{TS} in kcal mol^{-1}) and unimolecular rate coefficients k_{uni} (in s^{-1}) with the reaction energy (in kcal mol^{-1}).

Molecules	Pathway (3.1)		Pathway (3.2)		Reaction Energy
	ΔE^{TS}	k_{uni}	ΔE^{TS}	k_{uni}	(Final product - reactant)
CH_3OOOH	55.1	2.4×10^{-28}	6.4	1.4×10^{9}	-54.7
R^1-OOOH	62.7	6.8×10^{-34}	7.7	1.5×10^{8}	-46.4
R^4-OOOH	52.0	4.8×10^{-26}	6.4	2.5×10^{9}	-49.5
R^5-OOOH	54.6	5.5×10^{-28}	9.6	1.1×10^{7}	-53.8

Thermodynamic data for the two decomposition pathways

Table S2 represents the unimolecular reaction energy (product-reactant) in terms of electronic energy and Gibbs-free energy (both in kcal mol^{-1}) associated with two main decomposition pathways studied in the work. They were calculated using DLPNO–CCSD(T)/aug-cc-pVTZ//ωB97X-D/6-31+G*. As pathway (1) deals with the fragmentation process leading to radical generation, the formation reaction energy is positively high due to higher product energy than that of the reactant. Although, thermodynamically unfavorable via a non-spontaneous channel, this pathway has favorable kinetics with rate coefficients competitive in the atmosphere. Considering the evolution of the molecular oxygen either on the triplet or singlet potential energy surface, the dissociation energy in the case of the pathway (2) shows distinguishable ranges both in terms of electronic energy and Gibbs free energy. The results exhibit that the reaction proceeding via a triplet potential energy surface is considerably more favorable than that of a singlet potential energy surface with a stark difference of over 25 kcal mol^{-1}. It is to be noted that the single-point corrected electronic energies of some of the products on the singlet potential energy surface have energies higher than those of the reactant energies.

Table S2: Zero-point energy corrected decomposition reaction energy (ΔE_d in kcal mol^{-1}) and Gibbs free energy ($\Delta G_d^{\#}$ in kcal mol^{-1}) for all the isomers. Note: the superscripts (1) and (3) under pathway (2) signify the electronic state of molecular oxygen taken into consideration while calculating the total product energy .

Molecules	Pathway (1)		Pathway (2)			
	ΔE_d	$\Delta G_d^{\#}$	$^3[\Delta E_d]$	$^3[\Delta G_d^{\#}]$	$^1[\Delta E_d]$	$^1[\Delta G_d^{\#}]$
HOOOH	29.4	20.4	-38.8	-38.8	-7.9	-15.3
CH_3OOOH	25.1	13.9	-29.9	-29.9	1.0	-8.0
R^1-OOOH	26.7	13.7	-31.7	-31.7	-0.8	-11.1
R^2-OOOH	26.6	14.5	-29.2	-29.2	1.8	-7.6
R^3-OOOH	27.0	14.2	-28.9	-28.9	2.0	-7.9
R^4-OOOH	26.1	13.2	-29.6	-29.6	1.4	-9.1
R^5-OOOH	26.3	14.8	-31.4	-31.4	-0.4	-9.4
R^6-OOOH	26.7	14.3	-27.8	-27.8	3.2	-6.9
R^7-OOOH	30.7	16.7	-30.1	-30.1	0.9	-9.8
R^8-OOOH	26.8	14.2	-32.0	-32.0	-1.1	-11.6

Table S3 presents the ZPE corrected barriers using augmented correlation consistent triple and quadrupole basis sets in DLPNO-CCSD(T) single point energy calculation.[7] Our benchmark results confirm that aug-cc-pVTZ basis set with DLPNO-CCSD(T) method is suitable when calculating transition state energies.

Table S3: Comparison of aug-cc-pVTZ and aug-cc-pVQZ basis sets with DLPNO-CCSD(T) method to calculate energy barrier (in kcal mol^{-1}) for CH_3OOOH system for the decomposition pathway (2). $E^{(TS-ROOOH)}$ is the transition state for one-step reaction and $E^{(TS-Complex)}$ is the transition state via complex ($CH_3O...HO_2$) intermediate. Note: zero-point energy correction has been calculated at the ωB97X-D/6-31+G* level.

Single-Point	$E^{(TS-ROOOH)}$	$E^{(TS-Complex)}$	Reference
DLPNO-CCSD(T)/aug-cc-pVTZ	43.1	-	(Table 3)
DLPNO-CCSD(T)/aug-cc-pVQZ	43.6	-	
DLPNO-CCSD(T)/aug-cc-pVTZ	-	3.0	(Table 4)
DLPNO-CCSD(T)/aug-cc-pVQZ	-	2.7	

Clusters of hydrotrioxides consisting of multiple monomeric units

Molecular structures of hydrotrioxide clusters with three monomeric units are shown in Figure S3 and S4 and their respective single-point energy corrected Gibbs binding energies are presented in Table S4 along with the one computed at the DFT level of theory is presented at the Table S5. Table S4 in which the values computed at the high-level CCSD(T), quantum chemical method illustrates that the larger organic trioxide of ROOOH has a stronger binding capability than the methyl-trioxide moiety. This can be explained by the higher stabilization energy possessed by the larger trioxide, contributed by the high excess energy in the formation of ROOOH. However, it is very unlikely that the reaction cross section will be high enough to have reactions of trimer formation to be feasible in the atmosphere. At the same time, the trend of binding capabilities is in alignment with that of a cluster consisting of two molecular units (presented in the main text), where the ability to bond is higher in the case of acidic molecules than with the bases and neutral molecules.

Table S4: Gibbs free binding energy ($\Delta G_D^{Cluster}$ in kcal mol^{-1}) calculated at the DLPNO–CCSD(T)/aug-cc-pVTZ//ωB97X-D/6-31++G** level at 298 K of CH_3OOOH, and ROOOH with two monomeric units of other atmospheric relevant molecules. Note: MA : methylamine (CH_3NH_2), DMA : dimethylamine ($(CH_3)_2NH$), TMA : trimethylamine ($(CH_3)_3N$), SA : sulfuric acid (H_2SO_4), NA : nitric acid (HNO_3), and FA : formic acid (HCOOH).

Cluster type	CH_3OOOH	ROOOH
water	3.66	0.71
NH_3	3.85	1.82
MA	2.17	-0.14
DMA	0.34	-1.35
TMA	3.52	1.95
SA	-9.21	-14.96
FA	-9.38	-13.37
NA	2.99	-2.99

Table S5: Gibbs free binding energy ($\Delta G^{Cluster}$ in kcal mol^{-1}) calculated at the ωB97X-D/6-31++G** level at 298 K at 1 atm of CH_3OOOH, and ROOOH with two monomeric units of other atmospheric relevant molecules. Note: MA : methylamine (CH_3NH_2), DMA : dimethylamine ($(CH_3)_2NH$), TMA : trimethylamine ($(CH_3)_3N$), SA : sulfuric acid (H_2SO_4), NA : nitric acid (HNO_3), and FA : formic acid (HCOOH).

Cluster type	CH_3OOOH	ROOOH
water	0.48	-4.10
NH_3	0.38	-3.17
MA	-0.64	-4.10
DMA	-1.82	-4.85
TMA	1.97	-0.67
SA	-9.52	-17.26
FA	-12.48	-17.51
NA	1.66	-5.72

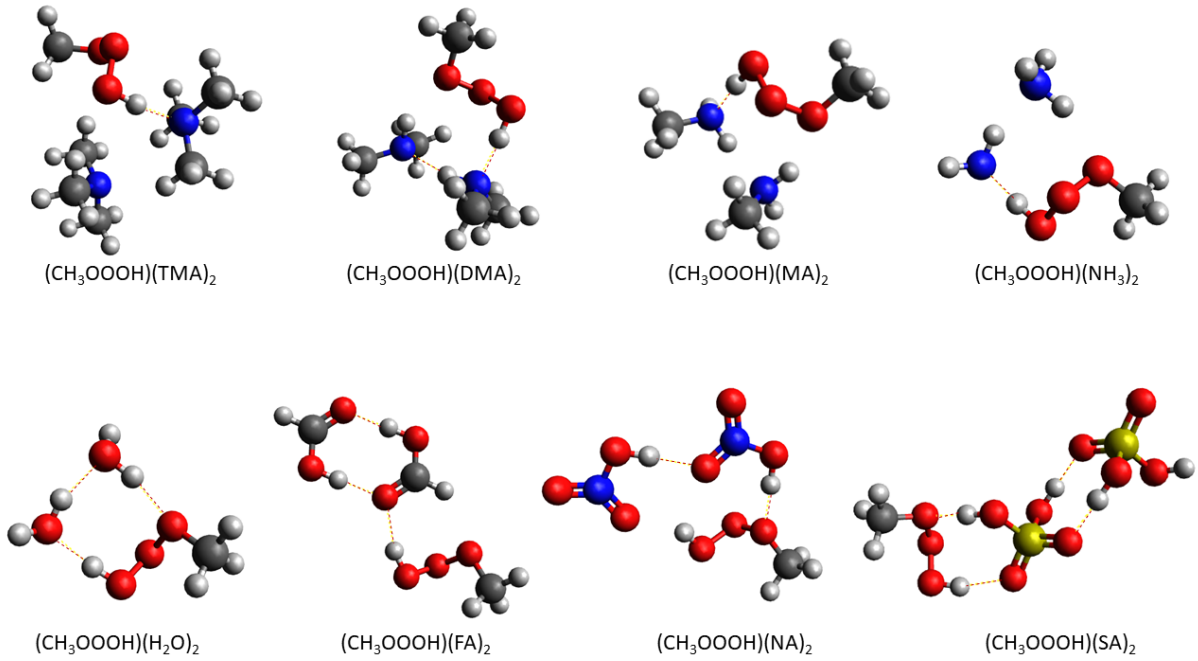

Figure S3: Global minimum molecular structures of clusters of CH_3OOOH with two other monomeric units of atmospheric relevant molecules viz water, NH_3, MA, DMA, TMA, SA, FA, NA, and self clustering. Color coding: brown is carbon, red is oxygen, blue is nitrogen, yellow is sulfur and white is hydrogen.

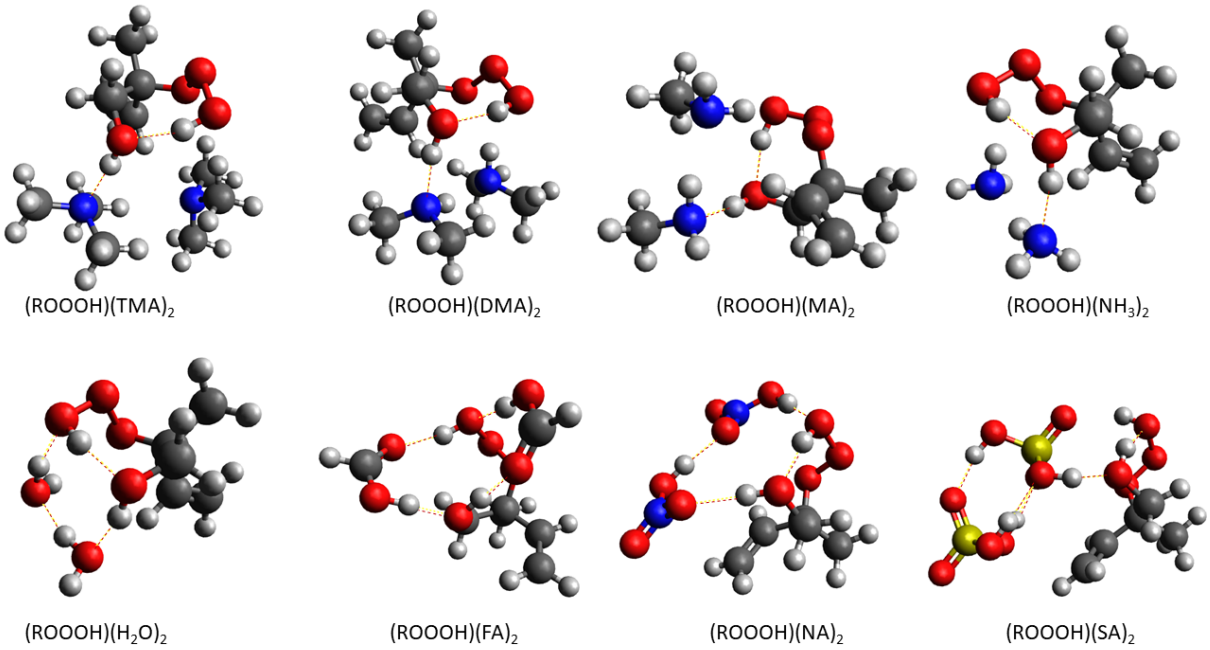

Figure S4: Global minimum molecular structure of clusters of ROOOH with two other monomeric units of atmospheric relevant molecules viz water, NH_3, MA, DMA, TMA, SA, FA, NA, and self clustering. Color coding: grey is carbon, red is oxygen, blue is nitrogen, yellow is sulfur and white is hydrogen.

Additionally, we perform clustering analysis of (a) CH_3OH, (b) $CH_3OO)H$, (c) CH_3OOOH and (d) ROOOH with two sets of sulfuric acid and ammonia cluster compositions viz $(SA)(NH_3)$ and $(SA)_4(NH_3)_4$. We can see from Table S6 that the trioxide (in general) has better binding capabilities than those of methanol and methyl-peroxide. Global-minimum molecular representations are illustrated in the Figure S5. Interestingly, the large difference in binding energy between CH_3OOOH and ROOOH, indicates the stability of the cluster is resulted from the size of the R- group dominantly. Due to limited computation sources, the binding energy of ROOOH and $(SA)_4(NH_3)_4$ is not presented here.

Table S6: Gibbs free binding energy ($\Delta G_D^{Cluster}$ in kcal mol^{-1}) calculated at the DLPNO–CCSD(T)/aug-cc-pVTZ//ωB97X-D/6-31++G** level of (1) CH_3OH, (2) CH_3OOH, (3) CH_3OOOH (4) ROOOH with $(SA)(NH_3)$ and $(SA)_4(NH_3)_4$ clusters. Note: SA is sulfuric acid (H_2SO_4).

Cluster type	CH_3OH	CH_3OOH	CH_3OOOH	ROOOH
$(SA)(NH_3)$	-0.95	-1.22	-2.2	-10.39
$(SA)_4(NH_3)_4$	1.94	0.12	-1.56	——

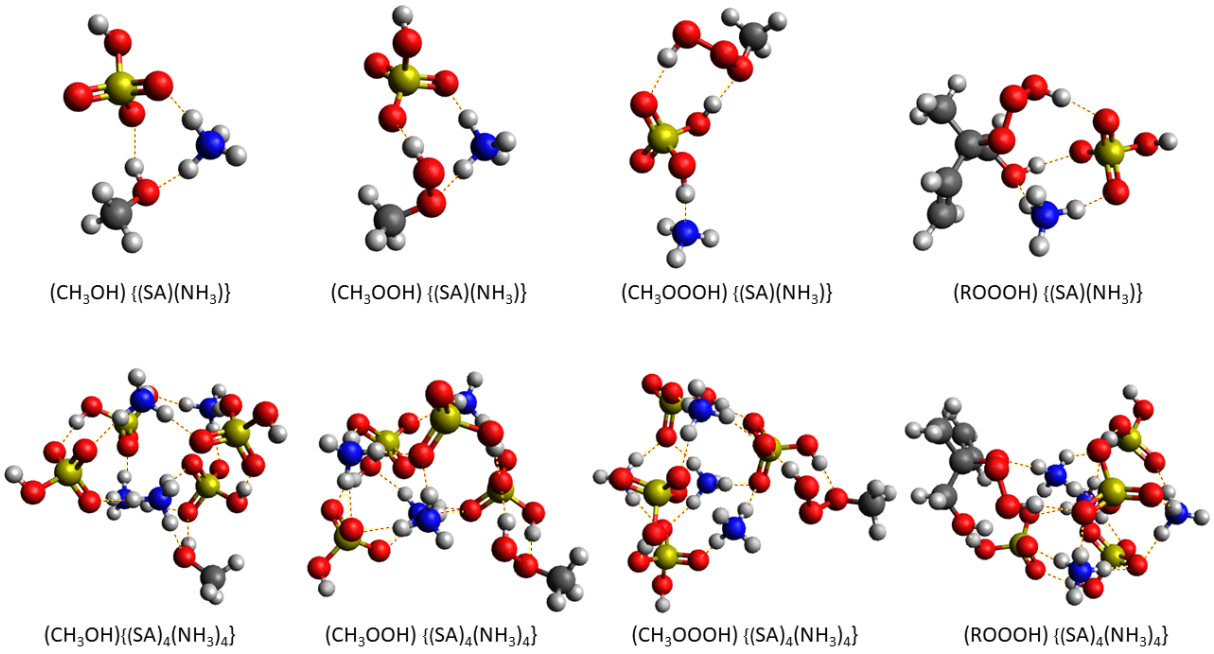

Figure S5: Global minimum molecular structure of clusters of CH_3OOOH and ROOOH with dimeric clusters of $(SA)(NH_3)$and $(SA)_4(NH_3)_4$. Color coding: grey is carbon, red is oxygen, blue is nitrogen, yellow is sulfur and white is hydrogen.

In Table S7, we present Gibbs binding free energies (calculated at ωB97X-D/6-31++G** level of theory) of all the atmospheric precursors taken into account for clustering analysis namely; CH_3OH, CH_3OOH, CH_3OOOH, and ROOOH with other atmospheric relevant systems.

Table S7: Gibbs free binding energy of dimers (in kcal mol^{-1}) consisting of CH_3OH, CH_3OOH, CH_3OOOH, or ROOOH with other atmospheric relevant systems.

Cluster type	CH_3OH	CH_3OOH	CH_3OOOH	ROOOH
water	2.24	2.45	1.37	-1.57
NH_3	0.60	-0.78	-1.42	-3.35
MA	-0.69	-0.52	-2.09	-4.17
DMA	0.34	-0.37	-2.45	-4.88
TMA	1.12	-0.78	-2.39	-4.52
SA	-4.23	-2.74	-3.04	-7.51
NA	-2.51	-0.59	-0.35	-5.00
FA	-5.84	-6.07	1.21	-4.70
self	1.43	1.50	1.07	-6.65
$(SA)(NH_3)$	-2.94	-2.38	-2.52	-8.31
$(SA)_4(NH_3)_4$	-1.19	-0.99	-1.84	-6.30

Lennard-Jones parameters for Master Equation calculations

Table S8: Lennard-Jones parameters σ and ε used for MESMER calculations for the pathway (1), and the relative electronic energies (R.E) calculated at the DLPNO–CCSD(T)/aug-cc-pVTZ//ωB97X-D/6-31+G* level of all the associated systems .

Molecules	σ (Å)	ε/k_B (K)	R.E (in kcal mol^{-1})	
			(ROO + OH)	(RO + HO_2)
HOOOH	4.5	437	29.4	29.4
CH_3OOOH	4.9	403	28.8	25.1
R^1-OOOH	5.9	541	29.7	26.7
R^2-OOOH	5.9	541	29.6	26.6
R^3-OOOH	5.9	541	29	27
R^4-OOOH	5.9	541	29.6	26.1
R^5-OOOH	5.9	541	29.4	26.3
R^6-OOOH	5.9	541	30.9	26.7
R^7-OOOH	6	629	29.9	30.7
R^8-OOOH	6	629	28.7	26.8

References

[1] E. Assaf, C. Schoemaecker, L. Vereecken and C. Fittschen, Experimental and theoretical investigation of the reaction of RO2 radicals with OH radicals: Dependence of the HO2 yield on the size of the alkyl group, *International journal of chemical kinetics*, 2018, **50**, 670–680.

[2] Y. Georgievskii and S. J. Klippenstein, Long-range transition state theory, *The Journal of chemical physics*, 2005, **122**, placeholder.

[3] P. J. Stephens, F. J. Devlin, C. F. Chabalowski and M. J. Frisch, Ab initio calculation of vibrational absorption and circular dichroism spectra using density functional force fields, *The Journal of physical chemistry*, 1994, **98**, 11623–11627.

[4] A. L. Hickey and C. N. Rowley, Benchmarking quantum chemical methods for the calculation of molecular dipole moments and polarizabilities, *The Journal of Physical Chemistry A*, 2014, **118**, 3678–3687.

[5] T. Berndt, J. Chen, E. R. Kjærgaard, K. H. Møller, A. Tilgner, E. H. Hoffmann, H. Herrmann, J. D. Crounse, P. O. Wennberg and H. G. Kjaergaard, Hydrotrioxide (ROOOH) formation in the atmosphere, *Science*, 2022, **376**, 979–982.

[6] J.-F. Müller, Z. Liu, V. S. Nguyen, T. Stavrakou, J. N. Harvey and J. Peeters, The reaction of methyl peroxy and hydroxyl radicals as a major source of atmospheric methanol, *Nature communications*, 2016, **7**, 13213.

[7] D. E. Woon and T. H. Dunning, Gaussian basis sets for use in correlated molecular calculations. III. The atoms aluminum through argon, *The Journal of Chemical Physics*, 1993, **98**, 1358–1371.